THE JOURNAL OF BIOLOGICAL CHEMISTRY
Vol. 274, No. 52, Issue of December 24, pp. 37443–37449, 1999

Printed in U.S.A.

His^{73}, Often Methylated, Is an Important Structural Determinant for Actin

A MUTAGENIC ANALYSIS OF HIS^{73} OF YEAST ACTIN*

(Received for publication, September 10, 1999, and in revised form, October 3, 1999)

Xiaoyi Yao, Stephanie Grade, Willy Wriggers‡§, and Peter A. Rubenstein¶

From the Department of Biochemistry, University of Iowa College of Medicine, Iowa City, Iowa 52242 and the ‡Department of Chemistry and Biochemistry, University of California, San Diego, California 92093

His^{73}, has been proposed to regulate the release of P_i from the interior of actin following polymerization-dependent hydrolysis of bound ATP. Although it is a 3-methylhistidine in the vast majority of actins, His^{73} is unmethylated in *S. cerevisiae* actin. We mutated His^{73} in yeast actin to Arg, Lys, Ala, Gln, and Glu and detected no altered phenotypes associated with the mutations *in vivo*. However, they significantly affect actin function *in vitro*. Substitution of the more basic residues resulted in enhanced thermal stability, decreased rate of nucleotide exchange, and decreased susceptibility to controlled proteolysis relative to wild-type actin. The opposite effects are observed with the neutral and anionic substitutions. All mutations reduced the rate of polymerization. Molecular dynamics simulations predict a new conformation for the His^{73} imidazole in the absence of a methyl group. It also predicts that Arg^{73} tightens and stabilizes the actin and that Glu^{73} causes a rearrangement of the bottom of actin's interdomain cleft leading possibly to our observed destabilization of actin. Considering the exterior location of His^{73}, this work indicates a surprisingly important role for the residue as a major structural determinant of actin and provides a clue to the impact caused by methylation of His^{73}.

His^{73} is conserved in all actins studied to date, and in the vast majority of actins, this residue is post-translationally methylated to produce *N*-τ-3-methylhistidine. The only exception to this rule had been the actin from *Naegleria gruberii* (1). However, we recently demonstrated that the actins from the yeasts *Saccharomyces cerevisiae* and *Candida albicans* were also nonmethylated (2). This residue lies on the outside of the protein in a cleft between subdomains 2 and 4 as part of a section of elongated polypeptide that extends downward from the top of subdomain 2 (Fig. 1). Based on the structure of skeletal muscle α-actin and nonmuscle β-actin which have methylhistidines, His^{73} is adjacent to a glutamic acid at position 72 and lies across the cleft from Asp^{184} in subdomain 4 (3–5). The conservation of a positively charged residue at this position suggests it might be necessary to offset the high negative charge density in the vicinity which otherwise might disrupt actin structure. Previously, we demonstrated that mutation of His^{73} in muscle actin would not prevent the incorporation of radiolabeled mutant monomers into wild-type actin filaments *in vitro* (6). However, in this case, it was entirely possible that the constraints imposed upon the mutant monomer by the WT[1] monomers in the filament masked any effects that the mutation would have caused in a pure mutant filament.

Based on molecular dynamics simulations, Wriggers and Schulten (7) have proposed that the imidazole moiety of this histidine residue blocks the opening of a channel by which water can gain access into the interior of the actin molecule where the bound nucleotide resides (7). This imidazole is over 6.5 Å away from the γ-phosphate of the bound ATP and is thus too far away to directly interact with the phosphate. However, these investigators subsequently proposed that following scission of the βγ-phosphate bond during polymerization, movement of the P_i away from the ADP toward the outside of the channel would allow it to interact with a positively charged imidazole thereby stabilizing the phosphate's negative charge. The interaction between the two moieties, promoted by protonation of the imidazole, would retard the release of the phosphate from the actin (8). Since the state of the nucleotide in the filament determines filament stability (9–11), this phosphate retention hypothesis, if correct, suggests that His^{73} might be an important factor in controlling cytoskeletal dynamics.

To investigate the effect of His^{73} on actin function, we have mutated this residue in *S. cerevisiae* actin. Substitution with Arg and Lys maintains a positive charge at this position, substitution with Ala neutralizes the charge. Replacement with Glu introduces a negative charge in place of the original positive charge, and finally substitution of Gln gives a neutral substitution isosteric with Glu. We have isolated yeast cells expressing each of these as the only actin in the cell and have assessed the effects of these mutations *in vivo*. Prior to assessing the mutations' effects on ATP hydrolysis and P_i release in terms of the phosphate-release model, it was necessary to determine the effects of the mutations on actin monomer integrity and polymerizability. We have thus isolated the actins and characterized the effects of the mutations on monomer stability, tertiary structure, nucleotide exchange, and the ability to form filaments at different temperatures. The results of these studies are reported here.

MATERIALS AND METHODS

The site-directed mutagenesis kit was purchased from Stratagene Corp. Oligodeoxynucleotides used for site-directed mutagenesis were synthesized in the DNA Core Facility at the University of Iowa. The

* This work was supported in part by National Institutes of Health Grant GM33689 (to P. A. R.). The costs of publication of this article were defrayed in part by the payment of page charges. This article must therefore be hereby marked "*advertisement*" in accordance with 18 U.S.C. Section 1734 solely to indicate this fact.

§ Supported in part by National Institute of Health grants to Ronald A. Milligan (Scripps Research Institute) and J. Andrew McCammon, (University of California, San Diego) and by the La Jolla Interfaces in Science Interdisciplinary Training Program/Burroughs Wellcome.

¶ To whom correspondence should be addressed: Dept. of Biochemistry, University of Iowa College of Medicine, Iowa City, IA 52242. Tel.: 319-335-7911; Fax: 319-335-9570.

[1] The abbreviations used are: WT, wild-type; Me, methyl.

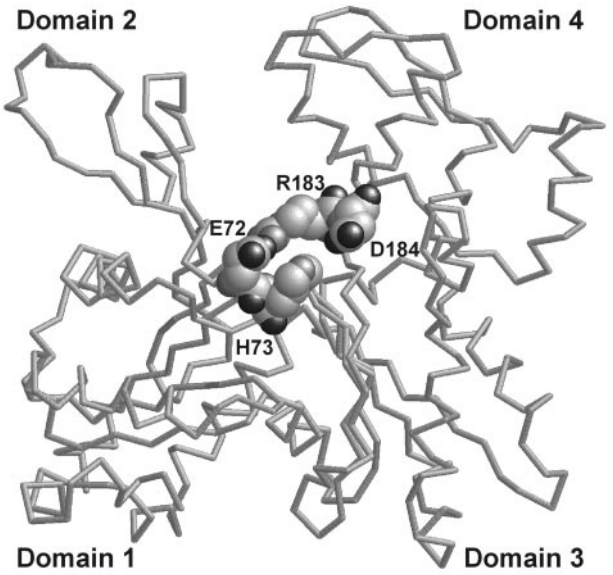

FIG. 1. **Position of His[73] in the actin monomer.** Shown is a polypeptide backbone three-dimensional structure of skeletal muscle actin with specific residues depicted using a space-filling mode. The figure was generated using the program Rasmol.

Sequenase Version 2.0 DNA sequencing kit was purchased from Sigma. DNase I was obtained from Worthington. Affi-Gel 10 was obtained from Bio-Rad. Etheno-ATP, α-chymotrypsin, trypsin, and subtilisin were purchased from Sigma.

Oligonucleotide-directed Mutagenesis—Site-directed mutagenesis was used to construct a mutant actin sequence carried in a centromeric vector pRS314 (12) marked with the *TRP1* gene. The oligodeoxynucleotide 5′-GGTTACCCAATTGAAC(G/A)A(C/G)A(T)GGTATTGTCACCAACTGG-3′ was used to generate the mutant actins in which the codon for His(CAC) was mutated to that for Ala(GCT), Gln(CAA), Glu(GAA), Lys(AAA), and Arg(CGT). The underlined sequences are the mutated codons. The DNA was sequenced in each case to verify the desired mutation.

Generation of Cells Producing Mutant Actins—pRS314 plasmids containing the mutant coding sequences were introduced into a *trp1,ura3-52* haploid cell in which the chromosomal *ACT1* gene had been disrupted by replacement of the coding sequence with the *LEU2* gene. Wild-type actin was expressed in these recipient cells from another centromeric plasmid containing the *URA3* gene. Following transformation with the mutant plasmid and selection on tryptophan-deficient medium, surviving cells were subjected to plasmid shuffling to eliminate the plasmid carrying the WT actin gene. The mutant plasmid was rescued from surviving trp^+,ura^- cells and sequenced to ensure that the mutation was still intact. Viable cells were readily obtained for all mutants.

Purification of Yeast Wild-type and His[73] Mutant Actins—Wild-type and His[73] mutant actins were purified using a combination of DNase I affinity chromatography, DEAE cellulose chromatography, and subsequent polymerization-depolymerization cycling as described previously (13). Calcium/G-actin was stored in calcium/G-buffer (10 mM Tris-HCl, pH 7.5, 0.2 mM $CaCl_2$, 0.2 mM ATP, and 0.5 mM dithiothreitol). Calcium/actin was converted to the magnesium form by treatment with 0.2 mM EGTA in the presence of 0.1 mM $MgCl_2$ at 25 °C for 10 min as described by Chen and Rubenstein (14) and Pollard (15). Magnesium/G-actin was used immediately after the conversion from calcium/G-actin. Actins were stored at 4 °C following purification and used within 4 days.

Actin Polymerization—Actin polymerization was assessed by the increase in light scattering that occurred following the addition of 2 mM $MgCl_2$ and 50 mM KCl to a G-actin solution in the thermostatted cuvette chamber of a Spex Fluorolog 3 fluorescence spectrometer. Excitation and emission wavelengths were set at 360 nm. For all experiments, wild-type actin was run as a control, and experiments were repeated with at least three different batches of actins. To assess cold sensitivity, actin was polymerized at 25 °C until a plateau was reached. The temperature was then lowered to 4 °C over a 15–30-min period of time and subsequently maintained at this temperature during which the change in light scattering was monitored.

Thermal Denaturation—The apparent melting temperatures of G-actins were determined by circular dichroism according to Chen and Rubenstein (14). 1.4 μM G-actin was heated at a constant rate of 1 °C/min over a range from 20 to 80 °C with constant stirring of the samples over the entire range tested. Changes in the ellipticity of actin samples were monitored at 222 nm in an AVIV 62 DS spectropolarimeter. Data were fitted to a two-state model with a single transition between a native and a denatured form of the protein and the T_m value was defined as the temperature when 50% of the G-actin was in the denatured form.

Nucleotide Exchange—Unbound ATP was removed from a 5 μM G-actin solution by gel filtration, and the actin was incubated with 0.3 mM etheno-ATP at 4 °C for 2 h. Excess nucleotide was removed by gel filtration. The subsequent actin solution was mixed with 0.1 mM ATP and the decay in fluorescence that accompanied release of the etheno nucleotide from the actin was monitored as a function of time with excitation and emission wavelengths at 340 and 410 nm, respectively. For rapid reactions, a stopped-flow fluorescence spectrometer was employed. Nucleotide exchange rates were derived by fitting the data to a single exponential expression.

Electron Microscopy—Actin (5 μM) polymerized at 25 °C was applied to carbon-coated Formvar grids and visualized following negaitve staining with 1.5% (w/v) uranyl acetate using a Hitachi 7000 electron microscope (University of Iowa Electron Microscope Facility).

Limited Proteolysis of G-actin—Alterations in the tertiary structure of G-actins were monitored by the susceptibility of the actins (9 μM) to limited digestion by the following three enzymes at the indicated actin/protease ratios (w/w): trypsin (80:1), subtilisin (400:1), and chymotrypsin (16:1) essentially as described previously (16). Incubations were carried out at room temperature for the desired time. The digestion with trypsin was stopped with 10 μg/ml trypsin inhibitor, and the digestion with the other two proteases was stopped with 1 mM phenylmethylsulfonyl fluoride. The samples were then separated by electrophoresis on a 12.5% SDS-polyacrylamide gel and visualized by staining with Coomassie Blue.

Molecular Modeling Studies—Molecular dynamics simulations of actin were carried out using the program X-PLOR (17) with the CHARMM-22 all-hydrogen force field (18). The structure of ATP-actin taken as the initial model was from the actin-gelsolin segment-1 complex (5), prepared with magnesium as divalent cation and solvated with 1,159 explicit water molecules as described in Ref. 8. The originally methylated MeHis[73] (5) was replaced by unmethylated histidine in three different protonation states (proton on the δ1 nitrogen or on the ϵ2 nitrogen or on both) for the control simulations, and by charged arginine and glutamate for the H73R and H73E mutants, respectively. The systems were subsequently refined by simulated annealing protocols. Simulated annealing is a conformational search technique that allows biomolecules to pass barriers between local minima in the complex energy landscape of proteins, faster than would be realized by simulations at room temperature. The method, thereby, accelerates the relaxation of the system from any less favorable interactions created by the mutation of His[73]. Simulated annealing protocols were successfully employed in earlier computational studies of kinesin (19) and apolipoprotein A-1 (20). Here we chose protocols of 170-ps length with a maximum temperature of 500 K.

RESULTS

Mutagenesis of His[73]—We wished to address the question of how His[73] affects the stability, tertiary structure, nucleotide exchange, and polymerization of actin. For this purpose, we used site-directed mutagenesis to substitute His[73] with Arg, Lys, Ala, Gln, and Glu and replaced the WT actin gene with the mutant actin genes in *S. cerevisiae* as described under "Materials and Methods." Viable haploid yeast cells producing only the desired mutant actins were readily obtained for each of the substitutions, and the presence of the desired mutation was confirmed by rescuing the plasmid from yeast and resequencing the DNA.

Effect of the His[73] Mutant Actins on Yeast in Vivo—To determine any defects caused by His[73] mutations *in vivo*, we first determined the growth rates of cells expressing each of the mutant actins. In liquid YPD medium at 10, 30, and 37 °C no appreciable difference was found between the generation times of each of the mutant cells and wild-type cells at the temperature tested (data not shown). Phase-contrast microscopy revealed no overt difference in either the size or morphology of the mutant cells compared with their wild-type counterpart. Calcofluor staining (21) showed that all the mutant cells displayed well formed chitin rings at the sites of previous budding

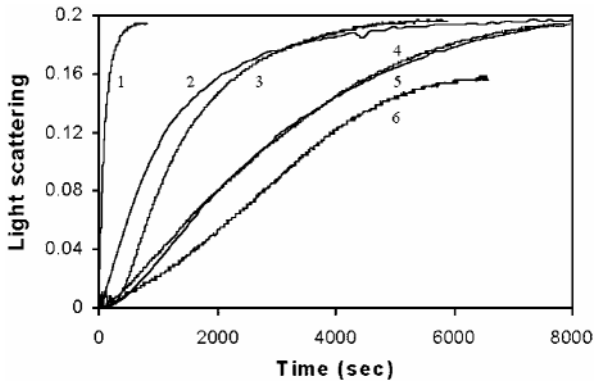

FIG. 2. **Polymerization of His[73] mutant actins at 25 °C.** Polymerization of the calcium form of each of the mutant and WT actins was induced by the addition of salt to the appropriate G-actin solutions as described under "Materials and Methods." The increase in light scattering due to polymerization was followed as a function of time. *Curve 1*, WT actin; *curve 2*, H73K; *curve 3*, H73R; *curve 4*, H73A; *curve 5*, H73Q; *curve 6*, H73E.

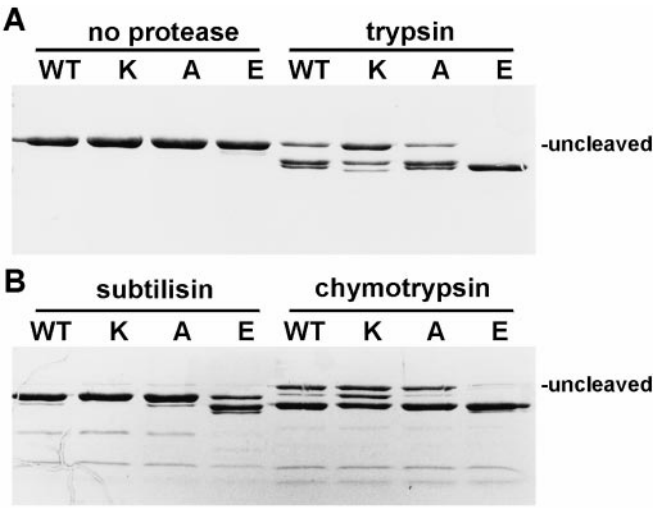

FIG. 3. **Protease susceptibility of His[73] mutant actins.** WT and His[73] mutant actins Lys, Ala, and Glu actins in the calcium/G form were subjected to controlled proteolysis as described under "Materials and Methods." After digestion, the samples were separated by electrophoresis on 12.5% SDS-polyacrylamide gels. *Panel A*, no protease; trypsin. *Panel B*, subtilisin; chymotrypsin.

events and the axial budding polarity typical of yeast (data not shown). To visualize the actin cytoskeleton directly, we stained wild-type and mutant cells with rhodamine/phalloidin (22). Again, there appeared to be no distinct difference in the phalloidin/staining patterns exhibited by mutant and WT cells in terms of the presence and distribution of cables and cortical patches.

Effects of His[73] Mutations on the Kinetics of Actin Polymerization at 25 °C—In order to interpret results obtained from phosphate release assays, we first had to assess the effects of these mutations on actin monomer structure and polymerizability. Fig. 2 shows the polymerization of the calcium form of each of the mutant and WT actins induced by the addition of salt to the appropriate G-actin solutions as described under "Materials and Methods." At 25 °C, each of the mutations had a noticeable effect on the rate of polymerization. The cationic substitutions, Lys and Arg, produced the mildest retardation in rates followed by Ala and Gln. The Glu mutation appeared to cause the most extensive retardation in polymerization.

Despite the slower polymerization of the mutant actins compared with WT actin, the extent of polymerization for all the actins except for H73E was essentially the same, suggesting that the critical concentrations of the mutant and wild-type actins are roughly identical. H73E might either have a higher critical concentration than wild-type or is less stable since the extent of polymerization of this mutant varies on a preparation to preparation basis between about 60 and 100%. Results with the magnesium form of the mutants showed the same relative order of effects, although in each case, the magnesium form of these actins polymerized faster than the corresponding calcium form. This has long been known to occur with WT actin. Finally, negatively stained polymerized samples of the Arg, Ala, Gln, and Glu mutations yielded filaments under the electron microscope with a morphology similar to that observed with WT actin.

The His[73] Mutations Alter the Conformation of Actin Subdomain 2—Subdomain 2 of G-actin, containing the DNase I loop, is a rather mobile structure, and the conformation of subdomain 2 and its transitions are important for actin function (23–26). Conformational changes in subdomain 2 can be probed by limited proteolysis with trypsin, subtilisin, and α-chymotrypsin. Trypsin cleaves subdomain 2 of calcium/G-actin at Arg[62]-Gly[63] and Lys[68]-Tyr[69], yielding 33-kDa C-terminal fragments. Subtilisin cleaves subdomain 2 of calcium/G-actin at Met[47]-Gly[48] and yields a 35-kDa fragment. α-Chymotrypsin cleaves subdomain 2 of calcium/G-actin at Met[44]-Val[45] and Leu[67]-Lys[68], producing 35- and 33-kDa fragments.

To determine the effects of the His[73] mutations on the conformation of subdomain 2 of G-actin, we carried out limited proteolysis of WT and His[73] mutant actins as described under "Materials and Methods." Fig. 3 shows that although controlled digestion of G-WT and G-His[73] mutant actins by trypsin, subtilisin, and α-chymotrypsin produced the same digestion patterns, the extent of digestion of H73K actin was less than that of its WT counterpart. In contrast, under the same conditions, the proteolysis of H73E actin appeared to be more extensive than that of its WT counterpart. These results indicate that the digestion sites of these proteases in subdomain 2 of H73K mutant actin are more protected and those of H73E mutant actin are more accessible than those of WT actin. H73R showed an even more protected pattern than H73K (data not shown). Thus, cationic substitutions appeared to confer greater resistance to proteolysis than that observed with WT actin and substitution of Glu for His[73] greatly increased susceptibility. Substitution of the neutral residue Ala produced a susceptibility roughly equivalent to that of WT actin. These results were observed with both the magnesium and calcium forms of actin although in all cases, the magnesium/G form is less susceptible than the calcium/G form, consistent with previous results.

ATP Exchange Rate of His[73] Mutant Actins—His[73] is located deep in the central cleft of the actin molecule, and the protease digestion sites of subdomain 2 are close to the top of the central cleft. If the His[73] mutations altered the conformation of the cleft around the nucleotide-binding site as suggested by the protease susceptibility studies, the changes might be manifested by altered rates of exchange of bound nucleotide from the actin. To address this hypothesis, we determined the ATP exchange rates of WT and His[73] mutant actins.

The Ala, Arg, Lys, and Gln mutations were assessed for their ability to exchange bound etheno-ATP for unbound ATP by monitoring the fluorescence of the bound etheno nucleotide as a function of time as described under "Materials and Methods." The results, shown in Fig. 4*A*, were obtained with all actins in the calcium form. The *inset* shows the H73R mutation on an extended time scale due to the extremely slow rate of exchange for this mutant actin. Initial attempts to measure the exchange of H73E were unsuccessful due to the rapid rate of exchange of this mutant. Its measurement was ultimately made on a

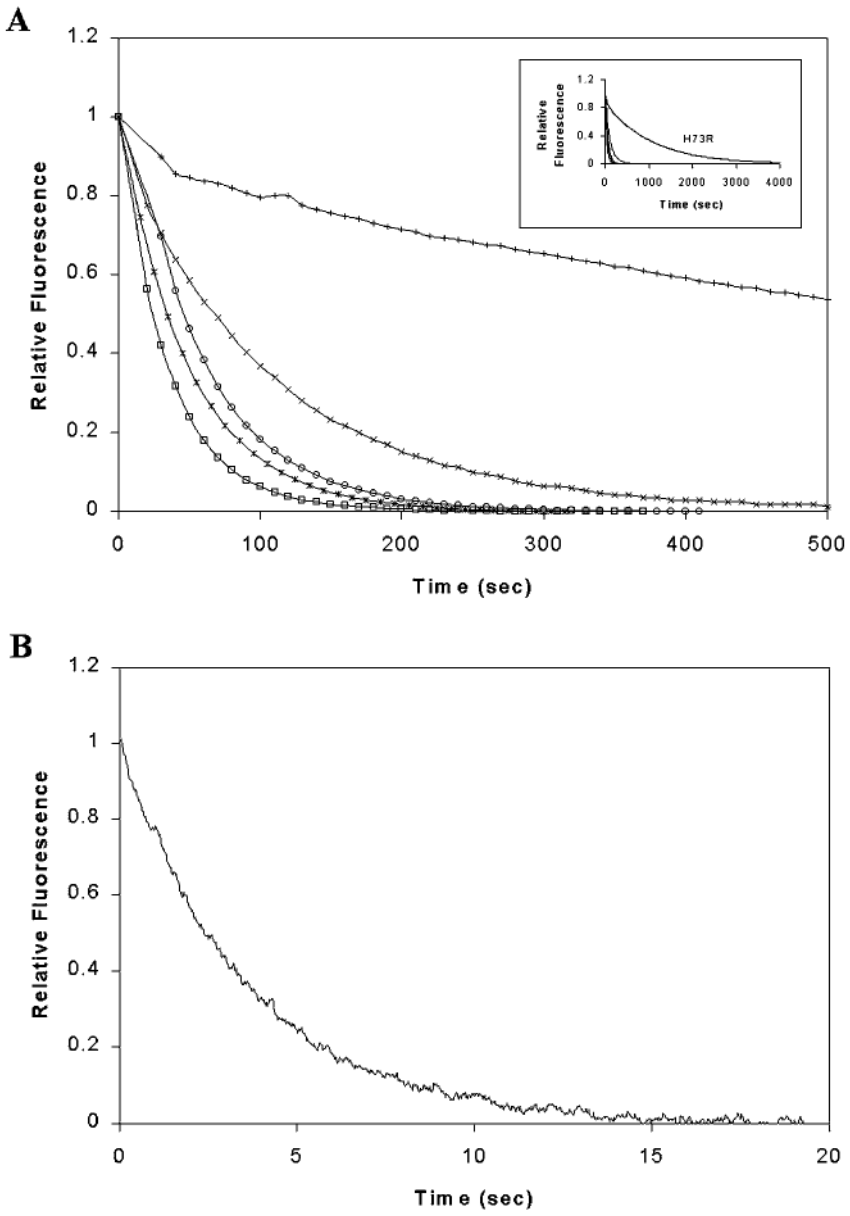

FIG. 4. **ATP exchange in His[73] mutant actins.** *A,* ATP exchange using H73A, Arg, Lys, and Gln actins. These mutants were assessed for their ability to exchange bound etheno-ATP for unbound ATP by monitoring the fluorescence of the bound etheno nucleotide as a function of time as described under "Materials and Methods." The *inset* shows the H73R mutation on an extended time scale due to the extremely slow rate of exchange for this mutant actin. ○, WT actin; *, H73A; □, H73Q; ×, H73K; +, H73R. *B,* ATP exchange of H73E actin. Due to the rapid rate of exchange of this mutant, the measurements were made on a stopped-flow fluorescence spectrometer.

stopped-flow fluorescence spectrometer (Fig. 4*B*). Exchange data for the mutants were fit to a first-order decay plot, and the $t_{½}$ values were calculated. Our results, shown in Table I, reveal that there is a hierarchy of effects of the different mutations on nucleotide exchange that correlates with the differences seen in protease susceptibility. The Arg substitution produces the longest delay compared with WT actin (almost ×20). Lys slows the exchange but to a much lesser extent than does Arg. Ala is slightly faster than WT as is Gln. Glu greatly accelerates the rate of exchange by about 14 times compared with WT actin. Thus, mutations which seem to produce a tighter, more compact monomeric structure also result in a retarded rate of nucleotide exchange while those which appear to open the structure accelerate the rate of exchange.

Thermal Stability of His[73] Mutant Actins—Our results so far have suggested that the basic residues result in a tighter, more compact monomer while the neutral and acid residues lead to a looser structure with greater conformational flexibility. To assess this situation further, we carried out circular dichroism experiments to determine the overall thermal stability of the His[73] mutant actins. The molar ellipticity at 222 nm, which reflects the content of α-helical structure in G-actin, was monitored as a function of temperature. The results are shown in Fig. 5. Based on the total change in dichroism, the degree of denaturation at each temperature was calculated and the data replotted as the fraction native *versus* temperature. The relative 50% denaturation value is defined as the apparent melting temperature (T_m) for the protein, and this value for each of the mutants is shown in Table II. The altered T_m value of all the mutants suggest that the nature of the substitution has a direct effect on the thermal stability of the actin monomer, even though residue 73 is on the exterior of the protein. Strongly cationic substitutions increase the stability of the protein over that of the WT protein whereas neutral substitutions cause slightly decreased stability. Substitution of glutamate greatly

TABLE I
$t_{1/2}$ values of ATP exchange of His[73] mutants
The exchange data for actins in the calcium form were fitted to a first-order decay plot and the $t_{1/2}$ values calculated.

	WT	H73A	H73Q	H73K	H73R
$t_{1/2}$ (s)	39	34	27	77	693

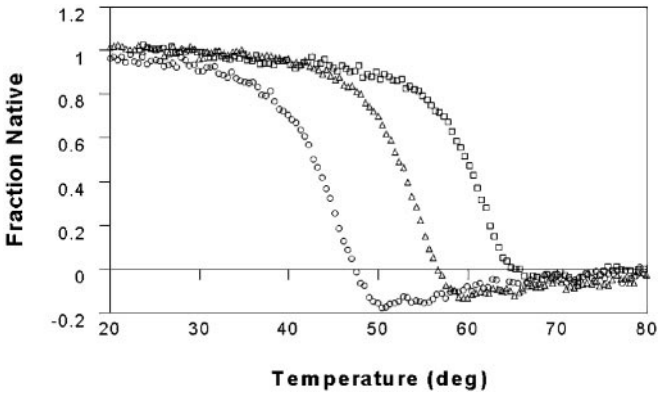

FIG. 5. **Thermal denaturation of His[73] mutants.** The thermal stability of the magnesium forms of WT, H73E, and H73R actins was assessed by subjecting G-actin solutions to increasing temperatures and monitoring the circular dichroism of the samples as a function of temperature as described under "Materials and Methods." Based on the total change in dichroism achieved, the degree of denaturation at each temperature was calculated and the data replotted as the fraction native *versus* temperature. ○, H73E; Δ, WT actin; □, H73R.

TABLE II
T_m values of His[73] mutant actins (°C)

Shown are the relative 50% denaturation temperatures for each of the His[73] mutant actins based on circular dichroism at 222 nm as described under "Materials and Methods."

	WT	H73A	H73Q	H73E	H73K	H73R
Magnesium actin	52	49	49	43	54	60
Calcium actin	59	58	56	53	61	66

destabilizes the protein. This gradient of results is consistent with our results from previous experiments.

Polymerization of Some His[73] Mutant Actins Is Cold-sensitive—One major interstrand force stabilizing the actin filament might be a "plug pocket" arrangement in which a hydrophobic plug at the tip of a loop between subdomain 3 and 4 interacts with a hydrophobic pocket formed by the interface of two subunits on the opposing strand of the helix (27, 28). Our previous work has shown that mutations in the hydrophobic plug produce effects consistent with a weakening of this proposed plug-pocket interaction and lead to disassembly of filaments at 4 °C (12, 29). Although residue 73 is not directly involved in the proposed interaction, it is on a strand of the polypeptide directly attached to the part of subdomain 2 hypothesized to be part of the "pocket." If alteration of the conformation around His[73] led to an altered conformation in these hypothetical pocket residues, the His[73] mutations might produce a "cold sensitivity" like that observed with the hydrophobic plug mutations.

Wild-type and mutant actins were polymerized at 25 °C. The temperature was then lowered to 4 °C, and the light scattering was monitored over time. Wild-type actin filaments were stable at 4 °C, as well as were the H73R and Lys filaments (data not shown). In contrast, the three other mutations H73A, Gln, and Glu resulted in actins that depolymerized at 4 °C (Fig. 6*A*). Glu always depolymerized completely while the Ala and Gln mutants showed about 80–90% depolymerization depending on the experiment. To determine the reversibility of this cold sensitivity, the temperature was returned to 25 °C in each of the cases, and polymerization was restored to almost the original level (Fig. 6*B*). Thus, cold-induced depolymerization did not result in irreversible changes in actin structure.

Molecular Modeling of WT, H73R, and H73E Actins—We next performed molecular modeling simulations on WT, H73R, and H73E mutant actins to determine if the absence of a methyl group on His[73] of yeast actin caused a realignment of

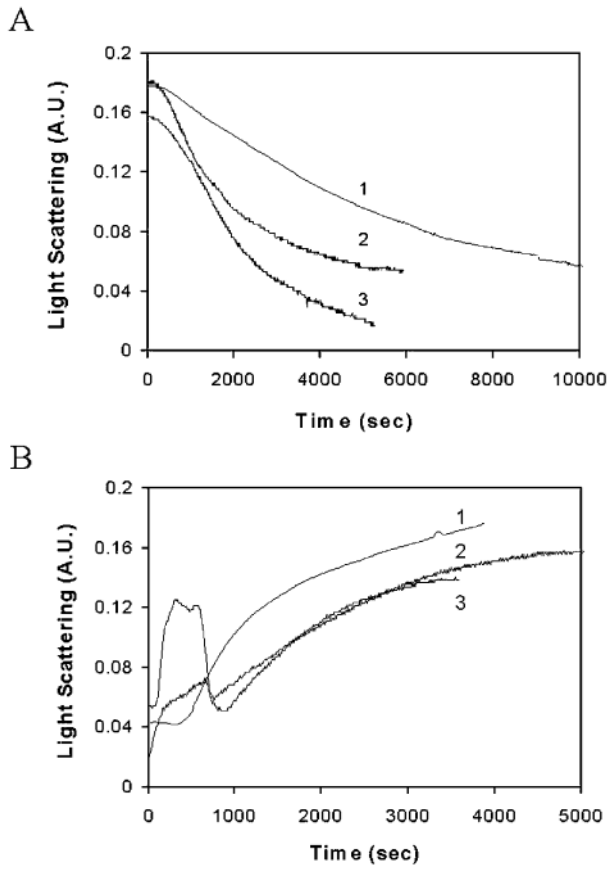

FIG. 6. *Panel A,* cold sensitivity assay of His[73] mutant actin polymerization. H73A (*curve 1*), Gln (*curve 2*), and Glu (*curve 3*) mutant actins (4 μM) were polymerized at 25 °C. The temperature was then lowered to 4 °C, and the light scattering was monitored over time. *Panel B,* following cold-induced depolymerization, the temperature was returned to 25 °C, and the increased in light scattering due to repolymerization was monitored. The curves are numbered as described in *panel A*.

residues at the bottom of actin's interdomain cleft. Also, we wished to better understand the molecular basis for the changes in actin behavior caused by these two His[73] mutations.

The methyl group on the ε2 nitrogen of MeHis[73], present in the crystal structure of muscle actin, was removed to simulate the WT state of yeast actin. The nonionized form of the imidazole ring can exist as two tautomers, with the proton on either the δ1 or ε2 nitrogens (30). The hydrogen is usually found on the ε2 nitrogen, but the pK_a of the δ1 atom is only about 0.6 pH unit lower than that of ε2. Thus, the position of the proton depends on the conditions of the local environment in the protein, and both forms may exist. Furthermore, histidine is readily protonated with a pK_a near 7, in which case the positive charge is shared by the two nitrogens by resonance. We have simulated all three charge states (proton on either atom or on both) starting with the crystal structure of the imidazole for a realistic modeling of the WT yeast actin.

Fig. 7, *A-D,* compares the three charge states of His[73] to the position of MeHis[73] in the crystal structure (5). In the cases where the δ1 nitrogen is protonated, the conformation of His[73] is close to that of MeHis[73] in the crystal structure regardless of the protonation state of ε2. The imidazole heavy atoms exhibit a root mean square deviation of only 0.7 and 0.9 Å from corresponding atoms in MeHis[73], for protonated and unprotonated ε2, respectively. The relative stability of these two cases is due to a δ1-proton-stabilizing hydrogen bond with the backbone oxygen of Gly[158] (hydrogen acceptor distances: 1.8 and 1.9 Å, donor hydrogen acceptor angles: 25 and 8°, for protonated and unprotonated ε2, respectively). In contrast, if ε2 alone is proto-

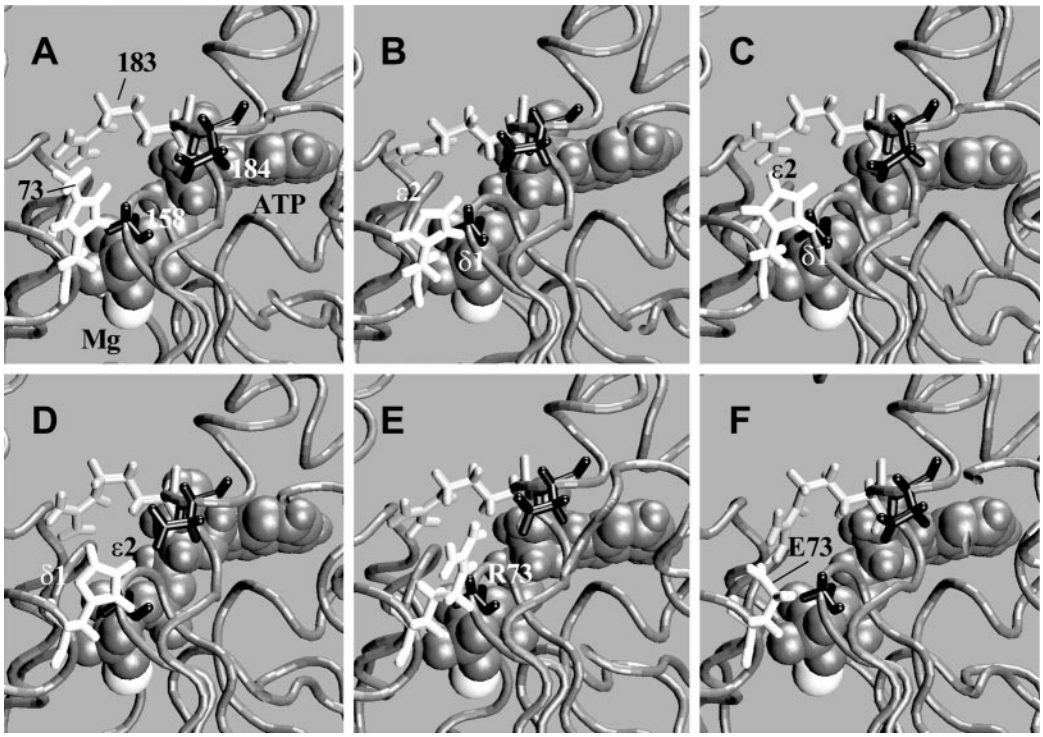

FIG. 7. **Structural models of actin depicting the effects of His[73] methylation and substitution by Arg and Glu.** Molecular dynamics simulations were performed and figures generated as described under "Materials and Methods." Depicted is the area around His[73] along with Gly[158], Arg[183], and Asp[184]. *A,* methylhistidine at residue 73; *B,* unmethylated His[73], δ1 proton is protonated; *C,* ϵ2 and δ1 nitrogens are both protonated; *D,* ϵ2 nitrogen only is protonated; *E*, H73R actin; *F,* H73E actin. In *panels B-D*, the imidazole is nonmethylated as is the case in yeast actin.

nated, the stabilizing hydrogen bond no longer exists, and the side chain flips about its long axis so that the proton on ϵ2 is oriented toward the carboxylate of nearby Asp[184] across the cleft separating the two domains of the protein. In this case, the imidazole exhibits a large root mean square deviation from MeHis[73] (1.8 Å), and a salt bridge is formed with Asp[184] (hydrogen acceptor distance: 1.9 Å, donor hydrogen acceptor angle: 11°).

The conformation of residue 73 in the two simulated mutants, Arg[73] and Glu[73], are depicted in Fig. 7, *E* and *F*, respectively. The positively charged side chain of Arg[73] coordinates both carboxylate oxygens of Asp[184] (hydrogen acceptor distances: 2.4 and 3.1 Å). On the other hand, Glu[73] does not form a salt bridge with Asp[184] but with Arg[183] (hydrogen acceptor distance: 1.7 Å, donor hydrogen acceptor angle: 16°). Residues 73, 183, and 184 are exposed to adjacent actin monomers in the WT filament (28), and their rearrangement in the Glu[73] mutant frees the negatively charged Asp[184] while neutralizing the positive charge on Arg[183].

DISCUSSION

Our results strongly suggest a role for this residue that is much more complex than simply controlling the rate of P_i release from actin as had been originally proposed. His[73] appears to be a major determinant of stability and conformational flexibility of the actin monomer despite the fact that it is located on the protein exterior where it can interact with solvent molecules.

First, our simulations of actin with His[73], as occurs in yeast, instead of the more common MeHis[73],predicted the possibility of a second conformational state for this residue and provide a potential clue as to the function of the methyl group found on His[73] in the vast majority of actins. This new state, expected to be pH and environment dependent, is stabilized by a salt bridge of the ϵ2 proton with Asp[184]. In contrast, the MeHis[73]-like state involves a weaker hydrogen bond between the δ1 proton and the Gly[158] oxygen. The salt bridge with Asp[184] would significantly stabilize the protonation of the ϵ2 and even that of the δ1 nitrogen. In T4 lysozyme, a similar salt bridge between residues Asp[70] and His[31] altered the pK_a values of these two residues from the normal values of 3.5 and 7 to 0.5 and 9, respectively (31) contributing 3–5 kcal/mol to the free energy of folding of the protein. Since we started with the crystal conformation that is stabilized by the weaker hydrogen bond, a transition to the salt bridge with Asp[184] was not observed in this work for doubly protonated His[73]. However, a tunneling through the singly ϵ2 protonated state would lower the barrier for the transition from the MeHis[73]-like conformation to the salt bridge conformation also for doubly protonated His[73]. This scenario is likely because ϵ2 protonation, that is, the state leading to salt bridge formation, is favored over δ1 protonation by the pK_a difference of the two nitrogens.

We have demonstrated that substitution at this residue with amino acids ranging from more basic to neutral and finally to an acidic residue produces a gradient of effects on actin structure and function. The magnitude and direction of these effects are consistent with the hypothesis that the imidazole of His[73] may interact electrostatically with nearby acidic residues, in particular Asp[184], on the opposite side of the interdomain cleft in actin to determine the range of movement of the two domains of actin relative to one another. Substitution of His[73] with strong cationic residues Arg and Lys seemed to result in a monomer with a tighter conformation as evidenced by a decreased nucleotide exchange rate, decreased rate of proteolysis of subdomain 2, and increased thermal stabilization. A plausible hypothesis is that the stronger positive charge allowed a more stable interaction with Asp[184] leading to a less flexible more protected interior of the monomer. The marked difference in effects of the Arg *versus* the Lys substitution might be due to the higher pK_a of Arg coupled with the lower flexibility of the

protein's side chain allow a stronger interaction to occur with Asp^{184}. The opposite effects were observed with H73E. These results suggest that charge repulsion with one of the acidic residues and subsequent rearrangement of amino acids at the base of the cleft results in a more open and flexible conformation responsible for the greatly enhanced rate of nucleotide exchange, greater protease susceptibility, and lower thermal stability.

The results of molecular modeling studies with the Arg and Glu mutants were consistent with the idea of an altered interaction involving Asp^{184}. Substitution of Arg produced a structure with a much stronger level of interaction predicted between the guanidinium group and Asp^{184} in the second state than would occur with His^{73}. This would lead to the hyperstabilization of the protein we observed experimentally. Substitution of Glu at residue 73 resulted in formation of a predicted salt-bridge between Glu^{73} and Arg^{183} with the concomitant breaking of a number of hydrogen bonds due to the resulting distortion of the tertiary structure of the protein. Interactions between residue 73 and 183 or 184 are likely to affect the stability of the actin fold since they link actin subdomains across the nucleotide binding cleft (3–5). In this context, the salt bridges formed by the Arg^{73} and Glu^{73} mutants are remarkable. The stronger bond formed by Arg^{73} would hyperstabilize contacts around the nucleotide leading to the effects we observed experimentally. Conversely, the Glu^{73}-Arg^{183} salt bridge would lead to a shift of the electrostatic charge on the surface of actin and alter the binding face and binding affinity to the adjacent monomer in the filament (28). Such a movement might easily alter the ATP-binding site leading to the enhanced nucleotide exchange kinetics, thermal instability, and the altered protease susceptibility we observed.

The observed polymerization kinetic effects with little if any change in critical concentration are consistent with our proposal of an electrostatic clamp near the base of the interdomain cleft. G-actin must undergo a conformational change to the F-monomer conformation before it can become incorporated into a growing filament (32). An increased interaction of residue 73 with Asp^{184} might result in the retardation of the rate at which this change occurs leading to slower polymerization. Elimination of the positive charge might impart enough increased conformational flexibility to make it easier for the protein to sample additional conformational states thereby retarding attainment of the F-monomer conformation. The rearrangement at the base of the cleft predicted with the Glu mutation might alter the rate at which the protein enters the F-monomer state resulting in even slower polymerization. However, the numerous inter-monomer contacts that develop during filament assembly might compensate for these altered monomer conformations with little net effect on critical concentration.

The cold-sensitive polymerization of the Ala, Glu, and Gln mutations but not the Arg and Lys species is intriguing. According to the hydrophobic plug-pocket proposal for filament stabilization, residues 63 and 64 along with residues 40–45 would constitute part of the hydrophobic surface that comprises the pocket in this interaction. Hydrophobic interactions are cold-sensitive, and we had previously demonstrated that mutations in plug residues resulted in cold-sensitive polymerization behavior. Neutralization of the positive charge at residue 73 produced an increased protease susceptibility in this region and moderate cold-sensitive behavior which was accentuated by substitution of an anionic residue. Altering the geometry of residues at the bottom of the interdomain cleft in actin likely results in a change of the surface at the top of subdomain 2. Such an alteration would cause a distortion in the pocket proposed by Holmes *et al.* (33), thereby decreasing the energy of the proposed hydrophobic interaction resulting in cold sensitivity. The smaller effect observed with the His^{73} mutations as opposed to that seen with the plug mutants may simply reflect the change in total hydrophobic surface that a single mutation in the plug makes relative to one in the larger pocket.

A second possible explanation is that His^{73} mutations alter the conformation of the plug in the same monomer by conformational changes propagated through the nucleotide bridge or interdomain cleft. However, the relatively large distance of the His^{73} imidazole from the ATP γ-phosphate coupled with the cold sensitivity of the neutral mutations despite their relatively small effect on monomer structure argues against this second possibility. In either case, the lack of a clear defective phenotype *in vivo* most probably reflects the fact that the conformational alterations produced by the mutations are at least in part cancelled by monomer-monomer interactions and the association of actin with different actin-binding proteins in the cell.

We originally wished to test the hypothesis that His^{73} regulates the rate of P_i release from F-actin following actin-catalyzed hydrolysis of ATP. However, from this study, His^{73} clearly plays an important role as a structural determinant of the actin monomer with concomitant effects on actin function. Therefore, one will have to be cautious in the interpretation of assays that may indicate a difference in the rate of P_i release from WT *versus* the His^{73} mutant species.

REFERENCES

1. Sussman, D. J., Sellers, J. R., Flicker, P., Lai, E. Y., Cannon, L. E., Szent-Gyorgi, A. G., and Fulton, C. (1984) *J. Biol. Chem.* **259,** 7349–7354
2. Kalhor, H. R., Niewmierzycka, A., Faull, K. F., Yao, X., Grade, S., Clarke, S., and Rubenstein, P. A. (1999) *Arch. Biochem. Biophys.,* **370,** 105–111
3. Kabsch, W., Mannherz, H. G., Suck, D., Pai, E. F., and Holmes, K. C. (1990) *Nature* **347,** 37–44
4. Schutt, C. E., Myslik, J. C., Rozycki, M. D., Goonesekere, N. C. W., and Lindberg, U. (1993) *Nature* **365,** 810–816
5. McLaughlin, P. J., Gooch, J. T., Mannherz, H. G., and Weeds, A. G. (1993) *Nature* **364,** 685–692
6. Solomon, L. R., and Rubenstein, P. A. (1987) *J. Biol. Chem.* **262,** 11382–11388
7. Wriggers, W., and Schulten, K. (1997) *Biophys. J.* **73,** 624–639
8. Wriggers, W., and Schulten, K. (1999) *Proteins Struct. Funct. Genet.* **35,** 262–273
9. Carlier, M.-F. (1991) *J. Biol. Chem.* **266,** 1–4
10. Carlier, M.-F., and Pantaloni, D. (1986) *Biochemistry* **25,** 7789–7792
11. Carlier, M.-F., Pantaloni, D., and Korn, E. D. (1984) *J. Biol. Chem.* **259,** 7349–7354
12. Chen, X., Cook, R. K., and Rubenstein, P. A. (1993) *J. Cell Biol.* **123,** 1185–1195
13. Cook, R. K., and Rubenstein, P. A. (1992) in *Practical Approaches in Cell Biology* (Carraway, K., and Carraway, C. C., eds) pp. 99–122, IRL Press, Oxford
14. Chen, X., and Rubenstein, P. A. (1995) *J. Biol. Chem.* **270,** 11406–11414
15. Pollard, T. D. (1986) *J. Cell Biol.* **103,** 2747–2754
16. Strzelecka-Golaszewska, H., Moraczewska, J., Khaitlina, S. Y., and Mossakowska, M. (1993) *Eur. J. Biochem.* **211,** 731–741
17. Brunger, A. T. (1992) *X-PLOR: A System for X-ray Crystallography and NMR,* Version 3.1, The Howard Hughes Medical Institute and Department of Molecular Biophysics and Biochemistry, Yale University, New Haven, CT
18. Brooks, B. R., Bruccoleri, R. E., Olafson, B. D., States, D. J., Swaminathan, S., and Karplus, M. (1983) *J. Comp. Chem.* **4,** 187–217
19. Wriggers, W., and Schulten, K. (1998) *Biophys. J.* **75,** 646–661
20. Phillips, J. C., Wriggers, W., Li, Z., Jonas, A., and Schulten, K. (1997) *Biophys. J.* **73,** 2337–2346
21. Pringle, J. R. (1991) *Methods Enzymol.* **193,** 732–734
22. Adams, A. E., and Pringle, J. R. (1991) *Methods Enzymol.* **194,** 729–731
23. Orlova, A., and Egelman, E. H. (1992) *J. Mol. Biol.* **227,** 1043–1053
24. Orlova, A., and Egelman, E. H. (1993) *J. Mol. Biol.* **232,** 334–341
25. Orlova, A., and Egelman, E. H. (1995) *J. Mol. Biol* **245,** 582–597
26. Orlova, A., and Egelman, E. H. (1997) *J. Mol. Biol.* **265,** 469–474
27. Holmes, K. C., Pop, D., Gebhard, W., and Kabsch, W. (1990) *Nature* **347,** 44–49
28. Lorenz, M., Popp, D., and Holmes, K. C. (1993) *J. Mol. Biol.* **234,** 826–836
29. Kuang, B., and Rubenstein, P. A. (1997) *J. Biol. Chem.* **272,** 1237–1247
30. Creighton, T. E. (1993) *Proteins*, 2nd Ed., pp. 13–14, W. H. Freeman and Co., New York
31. Anderson, D. E., Becktel, W. J., and Dahlquist, F. W. (1990) *Biochemistry* **29,** 2403–2408
32. Rich, S. A., and Estes, J. E. (1976) *J. Mol. Biol.* **104,** 777–792
33. Holmes, K. C., Popp, D., Gebhard, W., and Kabsch, W. (1990) *Nature* **347,** 44–49